JOURNAL OF SOLID STATE CHEMISTRY 62, 290–296 (1986)

A Neutron Powder Diffraction Study of the Low- and High-Temperature Structures of $Bi_{12}PbO_{19}$

A. D. MURRAY AND C. R. A. CATLOW

Department of Chemistry, University College London, 20 Gordon Street, London WC1, England

AND F. BEECH AND J. DRENNAN

Department of Metallurgy and Materials Science, Imperial College, Prince Consort Road, London SW7 2BP, England

Received June 14, 1985; in revised form August 27, 1985

We report the results of a high-resolution powder diffraction study of the low- and high-temperature structures of the compound $Bi_{12}PbO_{19}$. We find that at room and low temperatures a sillenite structure is adopted in which the anion vacancies are localized to specific locations on the sublattice. At high temperatures the material has a fluorite structure related to that of δBi_2O_3. We discuss the relationship between the structure of the material and its electrical characteristics. © 1986 Academic Press, Inc.

Introduction

The search for new materials displaying high oxygen ion conductivity has centered recently on doped derviatives of Bi_2O_3. One material that has attracted attention is $Bi_{12}PbO_{19}$ since, if as thought, it displays the sillenite structure (shown in Fig. 1) at room temperature, the potentially mobile vacancies would be an inherent part of the material. This means the problem of minimizing the binding between a dopant ion and its charge compensating vacancy population could be avoided. This would be reflected in a smaller activation energy for the defect motion and all other things being equal, high ionic conductivity values.

Our structural investigations of this material were motivated by the SIMS measurements of Kilner and co-workers (*1*) who suggested the existence of oxygen diffusion in the sillenite phase and, analogously to pure Bi_2O_3, a high-temperature phase transition to a phase displaying exceptionally high ionic conductivity. However, recent thermopower measurements performed by Chadwick and co-workers (*2*) on the low-temperature phases clearly show that the material displays purely electronic conductivity below the phase transition.

The aim of this present paper is to improve our knowledge of the properties of this material, by reporting the results of a high-resolution powder neutron diffraction study of both the low- and high-temperature phases of the material, and relating them to the measured electrical properties.

0022-4596/86 $3.00

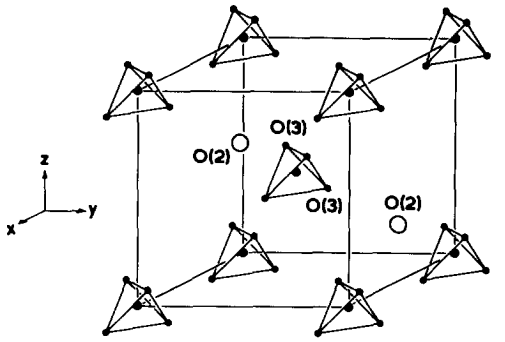

FIG. 1. Outline of one unit cell of $Bi_{12}PbO_{19}$ in the sillenite phase showing the tetrahedra around each (2*a*) site cation and the O(2) and O(3) positions.

Experimental

Samples were prepared by mixing the stoichiometric quantities of Johnson–Matthey Optran Grade PbO and Bi_2O_3 and firing in a gold crucible at 700°C for 15 hr. The samples were then re-ground and refired at 700°C for 24 hr. The powders were characterized by X-ray diffraction studies which confirmed them to be single phase. Extruded bars of the material were fabricated at 10 Tsi using a water binder, which was fired off at 300°C; the bars were densified over 48 hr at a temperature of 700°C.

The powder diffraction experiments were carried out on the high-resolution diffractometer D1A at ILL, Grenoble. Data were collected from 6° to 160° in 2θ at three temperatures, 5, 298, and 983 K. For the low-temperature studies the samples were contained in a 12-mm vanadium can, but for the high-temperature experiment the extruded bar was sealed in a quartz tube, contact between the sample and the quartz being prevented by gold foil.

A wavelength of 1.909 Å was used for the two lower temperature samples; while for the high-temperature experiment we used a wavelength of 1.384 Å in order to obtain more reflections from the higher symmetry structure. No assymetry in the peak shape due to the sintered nature of the sample was observed.

Preliminary processing of the data were carried out using the POWDER program written by Hewat (*3*). The profiles for the room and high-temperature samples are shown in Figs. 2a, b; the profile for the low temperature is similar to that for the room temperature study.

The data for the two lower temperatures were analyzed by the Rietveld profile refinement technique (*4*). The space group *I*23 was used as in the study of $Bi_{12}GeO_{20}$ by Abraham and co-workers (*5*). The data for the room temperature study were initially refined assuming lead occupation of the central (2*a*) site (see Fig. 1) with the bismuth being confined to the (24*f*) sites. The resulting refinement is given in Table I, a weighted profile reliability (*R*) factor of 5.37% was obtained. We note the large value (5.3 $Å^2$) obtained for the temperature

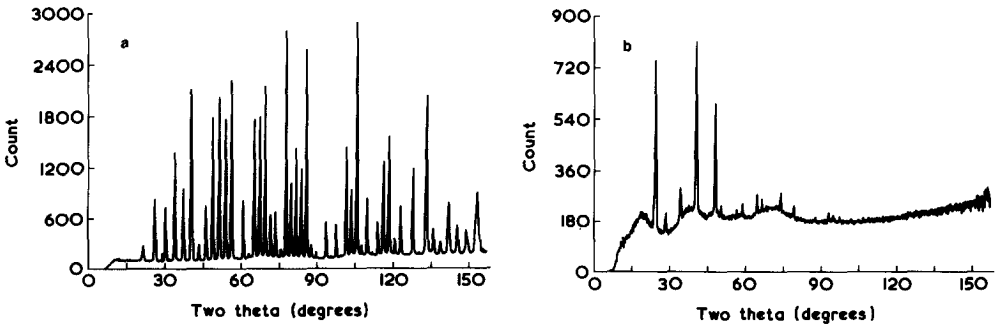

FIG. 2. (a) The room temperature diffraction pattern. (b) The 983 K diffraction pattern.

TABLE I

FINAL REFINEMENT VALUES FOR THE ROOM TEMPERATURE DATA SET ASSUMING CATIONS ON DISTINCT LATTICE SITES

Atom	Site	x	y	z	Occupation
Lattice parameter a = 10.2707(1)					
Pb	2*a*	0	0	0	2.0
Bi	24*f*	0.8231(1)	0.6787(1)	0.9832(1)	24.0
O(1)	24*f*	0.8652(2)	0.7510(2)	0.5125(2)	24.2(1)
O(2)	8*c*	0.8104(3)	0.8104(3)	0.8104(3)	8.1(1)
O(3)	8*c*	0.1097(3)	0.1097(3)	0.1097(3)	6.2(1)

Temperature factors

	B_{iso} (Å)^2	B_{11}	B_{22}	B_{33}	B_{12}	B_{13}	B_{23}
Pb	5.3(1)	—	—	—	—	—	—
Bi	—	0.0024(2)	0.0047(2)	0.0034(2)	0.0007(1)	−0.0006(2)	0.0007(2)
O(1)	—	0.0026(3)	0.0038(2)	0.0042(2)	0.0009(2)	−0.0014(3)	−0.0010(3)
O(2)	—	0.0037(3)	0.0037(3)	0.0037(3)	0.0006(2)	0.0006(2)	0.0006(2)
O(3)	—	0.0051(5)	0.0051(5)	0.0051(5)	−0.0011(2)	−0.0011(2)	−0.0011(2)

(Structure factor)^2	R = 2.09
Profile intensity	R = 5.25
Weighted profile	R = 5.37
Expected	R = 2.57

factor of the Pb^{2+} ion (which is constrained by symmetry to be isotropic); in contrast, normal values are observed for the temperature factors of the other atoms.

Unfortunately the scattering lengths of Pb^{2+} and Bi^{3+} are similar, and it is therefore difficult to obtain definite information on the distribution of Pb^{2+} over the (2*a*) and (24*f*) sites. However, a refinement in which a random distribution was assumed (using an average scattering length of 0.871 at both sites) yielded a slightly lower R factor of 5.28% although large temperature factors for the (2*a*) sites were still obtained. Refinement of the occupation numbers yielded no significant change; the refined O/M ratio is 1.485 ± 0.007 corresponding to a formula of $Bi_{12}PbO_{(19.3\pm0.1)}$. Full details of the refinement are given in Table II.

It was hoped that a clearer picture of the cation temperature factor behavior would emerge once thermal effects were minimized. The refinement details of the 5 K data set, assuming a random distribution of the cations, are listed in Table III. While the magnitude of the effect is substantially decreased it still persists to these low temperatures.

In contrast to the room temperature data, the profile obtained at 983 K contained only 15 reflections (corresponding to 13 intensities). The large Debye–Waller factors inherent at these temperatures in superionic materials results in such a reduction in scattering intensity that all reflections with 2θ greater than 100° were immeasurable. The structure is fcc and was refined in space group $Fm3m$. As the reflections are well spaced, profile refinement was unnecessary. The intensity data for each peak were integrated and refinement was carried out by the least-squares fitting program written by Wiseman (*6*).

Due to the highly modulated nature of the

TABLE II

FINAL REFINEMENT VALUES FOR THE ROOM TEMPERATURE DATA SET ASSUMING A RANDOM DISTRIBUTION OF CATIONS

Atom	Site	x	y	z	Occupation
Lattice parameter a = 10.2707(1)					
Pb/Bi	2*a*	0	0	0	2.0
Pb/Bi	24*f*	0.8231(1)	0.6786(1)	0.9829(1)	24.0
O(1)	24*f*	0.8651(2)	0.7510(2)	0.5122(2)	24.1(1)
O(2)	8*c*	0.8103	0.8103(3)	0.8103(3)	8.2(1)
O(3)	8*c*	0.1092(3)	0.1092(3)	0.1092(3)	6.3(1)

Temperature factors

	B_{iso} (Å)^2	B_{11}	B_{22}	B_{33}	B_{12}	B_{13}	B_{23}
Pb/Bi(2*a*)	4.2(1)	—	—	—	—	—	—
Pb/Bi(24*f*)	—	0.0024(2)	0.0049(2)	0.0034(2)	0.0008(2)	−0.0006(2)	0.0005(2)
O(1)	—	0.0029(3)	0.0038(2)	0.0041(3)	0.0009(2)	−0.0014(3)	−0.0008(3)
O(2)	—	0.0040(3)	0.0040(3)	0.0040(3)	0.0009(2)	0.0009(2)	0.0009(2)
O(3)	—	0.0050(5)	0.0050(5)	0.0050(5)	−0.0014(2)	−0.0014(2)	−0.0014(2)

(Structure factor)^2	R = 1.86
Profile intensity	R = 5.13
Weighted profile	R = 5.28
Expected	R = 2.57

TABLE III

FINAL REFINEMENT VALUES FOR THE 5 K DATA SET RANDOM DISTRIBUTION OF CATIONS

Atom	Site	x	y	z	Occupation
Lattice parameter a = 10.2401(1) Å					
Pb/Bi	2*a*	0	0	0	2.0
Pb/Bi	24*f*	0.8233(2)	0.6787(1)	0.9833(1)	24.0
O(1)	24*f*	0.8656(2)	0.7510(2)	0.5117(2)	24.0
O(2)	8*c*	0.8102(3)	0.8102(3)	0.8102(3)	8.1
O(3)	8*c*	0.1095(3)	0.1095(3)	0.1095(3)	6.2

Temperature factors

Atom	B_{iso} (Å)^2	B_{11}	B_{22}	B_{33}	B_{12}	B_{13}	B_{23}
Pb/Bi(2*a*)	3.3(1)	—	—	—	—	—	—
Pb/Bi(24*f*)		0.0014(3)	0.0025(2)	0.0008(2)	0.0006(1)	−0.0001(2)	0.0003(2)
O1		0.0014(4)	0.0017(3)	0.0016(3)	0.0003(3)	−0.0012(4)	−0.0013(3)
O2		0.0021(3)	0.0021(3)	0.0021(3)	0.0002(2)	0.0002(2)	0.0002(2)
O3		0.0017(5)	0.0017(5)	0.0017(5)	−0.0008(3)	−0.0008(3)	−0.0008(3)

background created by the quartz container the simplifying assumption of a flat background under a Bragg peak was used in the intensity summations. This approximation is of course not totally accurate although it is extremely difficult to assess the error limits introduced into the refinement using this assumption. We do not consider, however, that in our case the refinement has been biased to any significant extent.

In refining the data we assumed a random distribution of the two types of metal atom over the 4*a* (0,0,0) sites and of vacancies over the (8*c*) $(\frac{1}{4},\frac{1}{4},\frac{1}{4})$ sites.

Difference Fourier sections, however, revealed the presence of scattering density at the 32*f* (*x*,*x*,*x*) sites. The inclusion of the latter in the refinement resulted in the structure reported in Table IV for which an *R* factor of 2.5% was obtained. This level of information is as good as could be expected with the simple refinement model permissible on such a small number of independent reflections.

Discussion

Of paramount interest is the distribution of the anion deficiency. The two vacancies per unit cell; $Bi_{24}Pb_2O_{38+2\square}$ appear on the basis of the refinement to be constrained to occupy O(3) sites. This point is illustrated in Fig. 3. Refinements in which vacancies were introduced onto other crystallographic sites in the structure, in particular the O(2) position, were uniformly unsuccessful. The O(3)–(8*c*) site is associated with the tetrahedron around the *B* cation. It is tempting to speculate that the cation (either Bi^{3+} or Pb^{2+} since we cannot distinguish between them) has undergone *sp* orbital hybridization to create four sp^3 orbitals which one would expect to take tetrahedral coordination (*7*). The first three of these orbitals would be involved in bonding with the oxygen of the tetrahedron and the final one stabilizing the introduction of a vacancy into the lattice hence completing the tetrahedron.

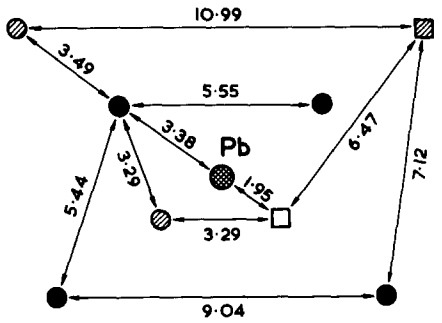

FIG. 3. The intersite distances for possible vacancy motions. ●, O(2); ⊘, O(3).

TABLE IV

FINAL REFINEMENT VALUES FOR THE 983 K DATA SET

Atom	Site	*x*	*y*	*z*	Occupation
Lattice parameter a = 5.64(1) Å					
Bi/Pb	4*a*	0	0	0	1.0
O(1)	8*c*	1/4	1/4	1/4	0.91(14)
O(3)	32*f*	0.36(1)	0.36(1)	0.36(1)	0.55(14)

Temperature factors

	B_{iso} (Å)^2
Bi	7.4(2)
O(1)	11.0(2)
O(2)	11.0(2)

(Structure factor)^2 R = 2.49

This kind of behavior has been examined in the work of Andersson (*8*) which has been continued by Galy and co-workers (*9*). They have shown that "lone pair" electrons are generally stereochemically active in that they often mimic the physical properties of an anion after adopting anion positions in a structure.

On this basis we can therefore qualitatively understand the large value of the temperature factor for the *B* cation, located at the center of the tetrahedron, as being the result of static displacements induced by the lone pair–vacancy interaction. The

magnitude of the smearing out of nuclear scattering density is indicated in Fig. 4. We should point out that in this case the center of electron density would be different from the nuclear center and hence no direct inference about the electron density distribution can be made.

We must now attempt to rationalize the defect structure with the measured electrical characteristics. Obviously we cannot offer a definitive explanation on the basis of our diffraction date in isolation. However, several important conclusions can be drawn from these data sets. The failure of attempts to introduce a vacancy population onto the O2 sites suggests that a cooperative vacancy jump mechanism between two BO_4 tetrahedra via an O2 site is unlikely.

There is of course the possibility of a vacancy jumping around an individual BO_4 tetrahedron; however, this would not result in long-range diffusional motion. If, then, we are restricted to vacancy–vacancy jumps then as is shown in Fig. 3 the distances involved are rather large.

We should like at this juncture to note the existence of a modulated background in the room temperature diffraction pattern (Fig. 2a). The extraction of definitive information about the nature of the short-range order causing this effect would require a long-wavelength diffuse scattering experiment.

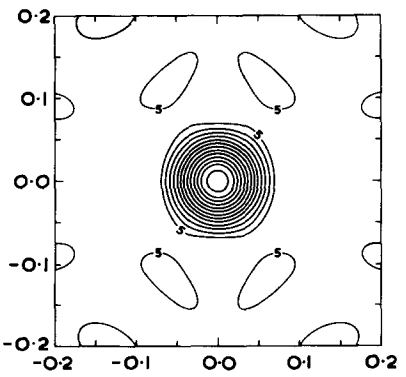

FIG. 4. The nuclear scattering density around a 2*a* site at 5 K.

Thus overall, it would appear that while the presence of "lone pair" cations in a material can lead to stabilization of vacancies on the anion sublattice, it is not axiomatic that the vacancies will be mobile. Indeed it would appear that the stabilizing interaction can act so as to trap the vacancy on the lattice site, thereby leading to significantly lower conductivities than those required for technological applications.

Similarly to pure bismuth oxide this material displays a high-temperature phase transition to an ionically conducting phase. However, due to the short temperature range that the phase is stable over and the reactive nature of the material at these temperatures little detailed experimentation has been performed on this phase. As discussed earlier the limited data sets that can be collected in powder diffraction experiments from high symmetry superionic materials at high temperatures precludes any sophisticated modeling of the defect structure although we should note that the structure of the high temperature phase of $Bi_{12}PbO_{19}$ is very similar to that reported by Battle and co-workers (*10*) for the δ phase of Bi_2O_3.

Summary and Conclusion

The work summarized in this paper has identified the basic structural features of the low-temperature phases of $Bi_{12}PbO_{19}$. It is apparent, however, that we are not yet in a position fully to describe the structure/conductivity phenomena in this material. Before any definitive solution of this problem can be achieved a more detailed understanding of the interaction between the cations and the vacancies is required, in particular, better information on the actual ion distribution on the sublattices than can be obtained from the average description provided by Bragg diffraction is needed. One approach to the problem would be a long-wavelength diffuse neutron scattering

experiment to investigate the possibility of macroscopic ordering on the anion sublattice coupled with an EXAFS study of the local environment around the cations. The EXAFS study should in principle be able to give detailed information on the Pb/Bi local environment hence revealing the microscopic distribution of the vacancies, thereby endowing us with a much more detailed description of the material.

Appendix: Definitions of *R* Factors

(Structure factor)^2

$$R = \frac{100 \sum_i \left| I_i^{obs} - I_i^{calc} \right|}{\sum_i \left| I_i^{obs} \right|}$$

Profile intensity

$$R = \frac{100 \sum_i \left| Y_i^{obs} - Y_i^{calc} \right|}{\sum_i \left| Y_i^{obs} \right|}$$

Weighted profile

$$R = \frac{100 \left(\sum_i W(Y_i^{obs} - Y_i^{calc})^2 \right)^{1/2}}{\left(\sum_i W(Y_i^{obs})^2 \right)^{1/2}}$$

Expected

$$R = \frac{100(N_f)^{1/2}}{\Sigma W(Y_i^{obs})^2}$$

where I_i^{obs} and I_i^{calc} are the observed and calculated peak intensities, Y_i^{obs} and Y_i^{calc} are the observed and calculated profile intensities, W is the weight of Y^{obs}, and N_f is the number of degrees of freedom.

References

1. J. A. KILNER, J. DRENNAN, P. DENNIS, AND B. C. H. STEELE, *Solid State Ionics* **5,** 527 (1981).
2. A. V. CHADWICK, E. S. HAMMAM, B. ZEQUIRI, AND F. BEECH, "The Kinetics and Mass Transport of Silicates and Oxide Systems," Materials Science Forum 7, 317–326 (1986) (R. Freer and P. Dennis, Eds.), Transtech (1985) (in press).
3. A. W. HEWAT, "The POWDER System for the Collation and Examination of Neutron Powder Diffraction Data," Internal Report, ILL, Grenoble.
4. J. M. RIETVELD, *J. Appl. Cryst.* **2,** 65 (1969).
5. S. C. ABRAHAMS, P. B. JAMIESON, AND J. L. BERNSTEIN, *J. Chem. Phys.* **47,** 4034 (1967).
6. P. WISEMAN, D. Phil. thesis, Oxford (1974).
7. R. J. GILLESPIE AND R. S. NYHOLM, Quat. Rev. **11,** 339 (1957).
8. S. ANDERSSON, AND A. ASTROM, *Nat. Bur. Std.*, Spec. Pub. 364, Proceedings of 5th Materials Research Symposium (1972), p. 3.
9. J. GALY, *Solid State Chem.* **27,** 284 (1979).
10. P. D. BATTLE, J. DRENNAN, C. R. A. CATLOW, AND A. D. MURRAY, *J. Phys. C* **16,** L561 (1983).